Journal of Volcanology and Geothermal Research 263 (2013) 132–140

Contents lists available at ScienceDirect

Journal of Volcanology and Geothermal Research

journal homepage: www.elsevier.com/locate/jvolgeores

Phase equilibria constraints on pre-eruptive magma storage conditions for the 1956 eruption of Bezymianny Volcano, Kamchatka, Russia

Vasily D. Shcherbakov [a,*], Owen K. Neill [b], Pavel E. Izbekov [b], Pavel Yu. Plechov [a]

[a] Department of Geology, Moscow State University, Moscow, Vorobievy Gory, 119899, Russia
[b] Geophysical Institute, University of Alaska Fairbanks, 903 Koyukuk Drive, Fairbanks, AK 99775-7320, USA

ARTICLE INFO

Article history:
Received 8 February 2012
Accepted 2 February 2013
Available online 26 February 2013

Keywords:
Phase equilibria
Bezymainny volcano
Andesite
Pre-eruptive conditions

ABSTRACT

Phase equilibria experiments were performed on andesites from the catastrophic 1956 eruption of Bezymianny Volcano, Kamchatka, Russia, to determine pre-eruptive magma storage conditions. Fifteen experiments were conducted under water-saturated conditions, with oxygen fugacity equal to the Ni–NiO oxygen buffer, at temperatures between 775 and 1100 °C and pressures between 50 and 200 MPa. Simultaneous amphibole and plagioclase crystallization is reproduced at ≤850 °C and ≥200 MPa. The simultaneous crystallization temperature range of the plagioclase–clinopyroxene–orthopyroxene–Fe–Ti oxide assemblage increases with decreasing pressure, from 840 to 940 °C at 150 MPa to 940–1020 °C at 50 MPa. Melt inclusion compositions in plagioclase phenocrysts and matrix glass match experimental melt compositions reproduced at 50–100 MPa and ≤50 MPa, respectively. Presence of the silica phase in groundmass and mature amphibole breakdown rims suggests that magma has been stored at ca. 3 km depth prior to the final ascent for at least 40 days. Syn-eruptive ascent led to decompression-driven crystallization, which caused a temperature increase from 850–900 °C to 950–1000 °C.

1. Introduction

Bezymianny Volcano is an andesitic stratovolcano located in the central Kamchatka Peninsula, which has been actively erupting almost continuously since its climactic eruption on March 30, 1956 (readers are directed to Girina, 2013, for a full review of this period). The 1956 eruption, marked by increasing seismic activity beneath the volcano, began on September 29th, 1955 (Gorshkov and Bogoyavlenskaya, 1965). Steam and ash emissions first appeared above the summit on October 22nd. Intensive ash falls, deformation of the edifice, and incandescence observed at the summit area during the night all indicated the injection of new juvenile magma within the edifice in the form of a cryptodome. Volcanic activity waxed and waned until the March 30, 1956 climactic event, when the collapse of the edifice produced a debris avalanche. In an eruptive sequence strikingly similar to that at Mount St. Helens in 1980 (Belousov et al., 2007, and references therein), this sudden collapse caused rapid decompression of cryptodome material and led to the formation of a directed lateral blast, followed by a few hours of vigorous explosive activity which generated a 35 to 40-km-high mushroom-shaped ash column, as well as extensive pyroclastic flows and lahars (Belousov, 1996). Juvenile material from the 1956 eruption is represented by grey high-density clasts and white low-density pumices. All juvenile clasts from the 1956 eruption are amphibole-bearing andesites, with remarkably similar bulk rock composition, mineralogy, and phenocryst contents (Belousov, 1996; Ozerov et al., 1997; Neill et al., 2010).

Previous authors have placed some constraints on magmatic storage conditions below Bezymianny. Based on earthquake distributions, Thelen et al. (2010) suggested the presence of an extended magma zone with a shallow storage region at 1–1.5 km depth and a deeper, larger magma body below 7–10 km. The latter is also suggested by the seismic study of Fedotov et al. (2010). Crystallization parameters of the Bezymianny andesites have been addressed in several petrological investigations (Kadik et al., 1986; Almeev et al., 2002; Plechov et al., 2008). The phase equilibria experiments of Kadik et al. (1986) suggest that the amphibole–pyroxene–plagioclase phenocryst assemblage of Bezymianny andesites originates from a deep magma storage region at pressures in excess of 300 MPa. The seismic and experimental petrology data on the Bezymianny plumbing system are consistent with high, bi-modal aluminum contents in amphiboles, suggesting their growth at two distinct pressure intervals of 200–300 MPa and 500–750 MPa (Turner et al., 2013). However, the low volatile contents in melt inclusions (Neill et al., in prep) and amphibole breakdown rims indicate that Bezymianny magma possibly resided at a depth much shallower than 7–10 km immediately prior to its final ascent and eruption.

Phase equilibria experiments are a technique commonly used to determine pre-eruptive magma storage conditions (e.g. Rutherford et al., 1985; Cottrell et al., 1999; Scaillet and Evans, 1999; Izbekov et al., 2004; Browne et al., 2010). This approach compares natural phase compositions and abundances with those synthesized in experimental runs at different experimental conditions. There are two fundamentally

* Corresponding author. Tel.: +7 9163205740.
E-mail address: vasiliy7@gmail.com (V.D. Shcherbakov).

0377-0273/$ – see front matter © 2013 Elsevier B.V. All rights reserved.
http://dx.doi.org/10.1016/j.jvolgeores.2013.02.010

different experimental approaches that consider crystal-melt equilibrium at different scales: (1) total equilibrium, in which chemical equilibrium is attained for all phases present in the system, and (2) local equilibrium, in which only a portion of the system is equilibrated (Pichavant et al., 2007 and references therein). Considering that natural magma reservoirs are prone to short-term perturbations and rarely return to a total equilibrium state, as evidenced by the frequent occurrence of disequilibrium features in volcanic rocks, the local equilibrium approach is often better suited for experimental replication of such systems. We use it in this study to determine the conditions at which magma last equilibrated prior to the 1956 catastrophic eruption at Bezymianny, thus providing additional constraints on the shallow Bezymianny plumbing system.

2. Samples and techniques

A fragment of white vesicular pumice from one of the last pyroclastic flows generated during the climatic phase of the March 30, 1956 eruption was used as starting material (Sample 05IPE24). Although the juvenile 1956 eruption material appears homogeneous in terms of bulk chemistry (Table 1), the composition of glass and the outermost rims of minerals differs slightly between dense and vesicular varieties (Neill et al., 2010). Because cryptodome rocks spent more than 2 months at near-surface pressures within the volcanic edifice prior to eruption, they are highly degassed and have crystallized to a degree far in excess of what would be expected in samples that did not spend significant time at the surface (Neill et al., 2010). We have purposely avoided using dense juvenile clasts as a starting material because they likely represent cryptodome magma that experienced this shallow-level crystallization. The sample used as starting material was crushed lightly to minimize breaking the phenocrysts and exposing their interiors to melt, and, consequently, to avoid any influence of compositional phenocryst inhomogeneity on phase equilibria. Such a technique is commonly used to investigate both pre-eruptive conditions (e.g. Rutherford and Devine, 1996; Pichavant et al., 2007) and late stages of crystallization (e.g. Hammer and Rutherford, 2002; Brugger and Hammer, 2010).

All experiments were conducted in the University of Alaska Fairbanks (UAF) experimental petrology laboratory. High-temperature experiments were carried out in tungsten–zirconium–molybdenum (TZM) pressure vessels, bathed in argon. The temperature in the hot core of the vessel was calibrated by K-type thermocouple immediately prior to experiments and was found to match previous temperature calibrations within ±2 °C. The temperature gradient in the hot core was measured repeatedly as part of the calibration routine and was found to be less than 1 °C/mm in the lowest 10 mm of the vessel. The positions of experimental sample assemblies within the hot core were controlled precisely to minimize the influence of the temperature gradient. We estimate that the overall temperature uncertainty of our experiments does not exceed 3–5 °C.

A mixture of argon and methane was used as a pressurizing medium, with pressure monitored by a factory-calibrated Heise gauge precise to ±0.4 MPa. Oxygen fugacity was held near NNO following the double-capsule approach, in which a mixture of Ni and NiO is isolated inside a platinum capsule within the sample assembly, crimped but not welded to allow vapor exchange between the buffer capsule and the experimental charge (Larsen, 2006). The addition of calibrated amounts of methane into pressurizing media allowed hydrogen to be generated at high temperature through methane breakdown ($CH_4 = 2H_2 + C$) and minimized the effect of hydrogen loss from the vessel, thus extending the lifespan of the oxygen fugacity buffer.

Sample assembly included a 4-mm-diameter $Au_{75}Pd_{25}$ capsule containing 70–120 mg of starting material, the solid buffer assembly, and a sufficient amount of de-ionized H_2O to saturate the melt and provide buffer action. The duration of high-temperature experiments varied from 7 to 13 hours. Each run was quenched almost instantaneously by flipping the pressure vessel and forcing the sample assembly to fall to the water-cooled end. After every experiment each sample was re-weighed to check for any weight loss. The solid buffer assembly was extracted and visually checked for the presence of both nickel and NiO. The presence of Ni was verified using a hand-held magnet, while NiO was identified visually by its distinctive green color. Experiments that lost water or/and failed to maintain oxygen fugacity at NNO were discarded.

Two low-temperature experiments were conducted in Renee-type pressure vessels using H_2O as a pressurizing medium. Oxygen fugacity was buffered by a nickel filler rod and pressure vessel material at NNO + 1 ± 0.5 log units (Geschwind and Rutherford, 1992; Gardner et al., 1995). Sample assembly consisted of 4-mm-diameter $Au_{75}Pd_{25}$ capsule containing 200–350 mg of starting material and a sufficient amount of de-ionized water to saturate the melt. Experiment duration was 96 hours (Table 2).

Major element analyses of minerals and glasses and acquisition of back-scattered electron (BSE) images were conducted at the University of Alaska, Fairbanks with a CAMECA SX-50 electron microprobe, equipped with one energy-dispersive spectrometer (EDS) and four wavelength-dispersive spectrometers (WDSs) and automated with ProbeForEPMA software (Donovan et al., 2007). The analytical conditions for plagioclase analyses included 15 kV accelerating voltage, 10 nA beam current, and 2 to 3-μm-diameter focused electron beam. Newly-grown pyroxenes and amphiboles were not large enough in size for quantitative analyses; these phases were identified by EDS only. Glasses were analyzed with a 10-μm diameter beam, utilizing the time-dependent Na-loss correction (Nielsen and Sigurdsson, 1981; Donovan et al., 2007). The deficit of totals of melt inclusion analyses was assumed to be due to the presence of water (Devine et al., 1995), and its effect on X-ray intensities was accounted for following Roman et al. (2006). BSE images were acquired at 20 kV accelerating voltage and 30 nA beam current. A few BSE images were acquired using a JEOL JSM-6480LV scanning electron microscope (SEM) at the Geological Department of the Moscow State University.

Table 1
Bulk rock composition of 1956 rocks.

Sample	SiO2	TiO2	Al2O3	Fe2O3	MnO	MgO	CaO	Na2O	K2O	P2O5
05IPE22a	60.47	0.58	17.88	6.62	0.15	2.56	6.61	3.47	1.26	0.19
05IPE23a	60.03	0.59	17.88	6.56	0.14	2.67	6.63	3.51	1.26	0.18
05IPE23b	60.16	0.6	17.79	6.77	0.14	2.73	6.64	3.47	1.26	0.18
05IPE24	59.95	0.59	17.86	6.59	0.14	2.71	6.65	3.45	1.25	0.18
06IPE9	61.02	0.58	17.75	6.42	0.14	2.62	6.5	3.61	1.32	0.18

3. Petrology and mineralogy of 1956 eruptive products

The March 1956 eruptive products are represented by various lithologies (Gorshkov and Bogoyavlenskaya, 1965; Belousov, 1996), which differ only in density and groundmass crystallinity (Neill et al., 2010). Based on 1500 point counts, the 1956 Bezymianny andesites used as a starting material in this study contain 21.4 vol. % of plagioclase phenocrysts, 3.4 vol. % of amphibole, 0.8 vol. % of orthopyroxene, 1.4 vol. % of Fe–Ti oxides, and 73.0 vol. % of groundmass (Fig. 1a). Amphibole and plagioclase are the predominant mineral phases; the size of their phenocrysts often exceeds 3 mm. Orthopyroxene and Fe–Ti oxides occur as 0.2–0.3 mm crystals, and compose less than 10% of the total phenocryst population. The groundmass is composed of plagioclase, orthopyroxene, Fe–Ti oxides, a silica phase, and rhyolitic glass (Fig. 1b). Clinopyroxene, apatite, zircon, and Cu–Fe sulfides are present in trace amounts.

Plagioclase phenocrysts are euhedral, tabular in shape, and exhibit polysynthetic twinning and complex compositional zoning. Plagioclase composition varies from 48 to 77 mol. % anorthite (An). Most phenocrysts consist of zones with nearly constant composition ($An_{50 \pm 5}$) and zones enriched in An up to An_{77} (Fig. 1c). The

Table 2
Experimental conditions and stable phases.

Name	Temperature (°C)	Pressure (MPa)	fO_2	Duration (hrs)	Pressure vessel	Phases present
BZ-2	775	200	NNO	165:15	Waspalloy	Gl, Plg, Opx, Amp, Mte, Ilm
BZ-1	850	100	NNO	163:20	Waspalloy	Gl, Plg, Opx, Mte
BZ-17	850	150	NNO	8:00	TZM	Gl, Plg, Opx, Cpx, Mte
BZ-19	850	200	NNO	7:20	TZM	Gl, Plg, Opx, Cpx, Amp, Mte
BZ-14	900	100	NNO	12:40	TZM	Gl, Plg, Opx, Cpx, Mte
BZ-20	900	200	NNO	7:40	TZM	Gl, Opx, Cpx
BZ-12	950	50	NNO	8:00	TZM	Gl, Plg, Opx, Cpx, Mte
BZ-4	950	100	NNO	10:45	TZM	Gl, Plg, Opx, Cpx, Mte
BZ-18	950	150	NNO	8:10	TZM	Gl, Opx
BZ-21	950	200	NNO	7:50	TZM	Gl, Opx
BZ-10	1000	50	NNO	7:25	TZM	Gl, Plg, Opx, Cpx, Mte
BZ-3	1000	100	NNO	8:00	TZM	Gl, Plg, Opx
BZ-11	1050	50	NNO	7:45	TZM	Gl, Plg, Opx, Mte
BZ-9	1050	100	NNO	7:40	TZM	Gl, Opx
BZ-7	1100	100	NNO	6:00	TZM	Gl

Gl = glass, Plg = plagioclase, Opx = orthopyroxene, Cpx = clinopyroxene, Amp = amphibole, Mte = magnetite, Ilm = ilmenite.

volumetric ratio of the two types of zones varies between individual phenocrysts. Although we did not attempt to quantify the ratio, zones with constant composition appear to dominate. A few crystals have dusty zones rich in fluid and melt inclusions. A portion of plagioclase phenocrysts contain high-An cores with abundant fluid and melt inclusions. The zoning patterns of plagioclase phenocrysts in 1956 samples generally resemble those found in the 2000–2007 eruptive products of Bezymianny Volcano (Shcherbakov et al., 2011).

Amphibole appears as brown and greenish-brown, euhedral, prismatic phenocrysts, whose length often exceeds 2 mm. All crystals are surrounded by 5 to 10-μm-thick reaction rims, which are considerably thinner than the reaction rims in cryptodome material (25–35 μm) found by Plechov et al. (2008). A few amphibole phenocrysts contain anhedral, high-Al, low-Mg cores (Fig. 1d), surrounded by rims containing lower Al and higher Mg. Total Al_2O_3 ranges from 8–15.4 wt.%. Please refer to Turner et al. (2013) for more details on amphibole composition.

Orthopyroxenes occur as euhedral, prismatic phenocrysts and microlites, and appear to be compositionally and texturally homogeneous with En content varying from 62 to 64 mol. %.

Fe–Ti oxides are represented by both titanomagnetite and ilmenite. The titanomagnetite is present as subhedral, equant phenocrysts and microlites, whose composition varies within 30–39 mol. % Usp. Ilmenites are rare and typically occur as tabular euhedral phenocrysts with ilmenite (Ilm) content ranging from 20 to 22 mol. %.

Matrix glass is rhyolitic and is characterized by relatively large variations in composition (Table 3). Silica content varies from 74.3 to 79.2 wt.% SiO_2 with a mean of 76.8 wt.%, while K_2O varies from

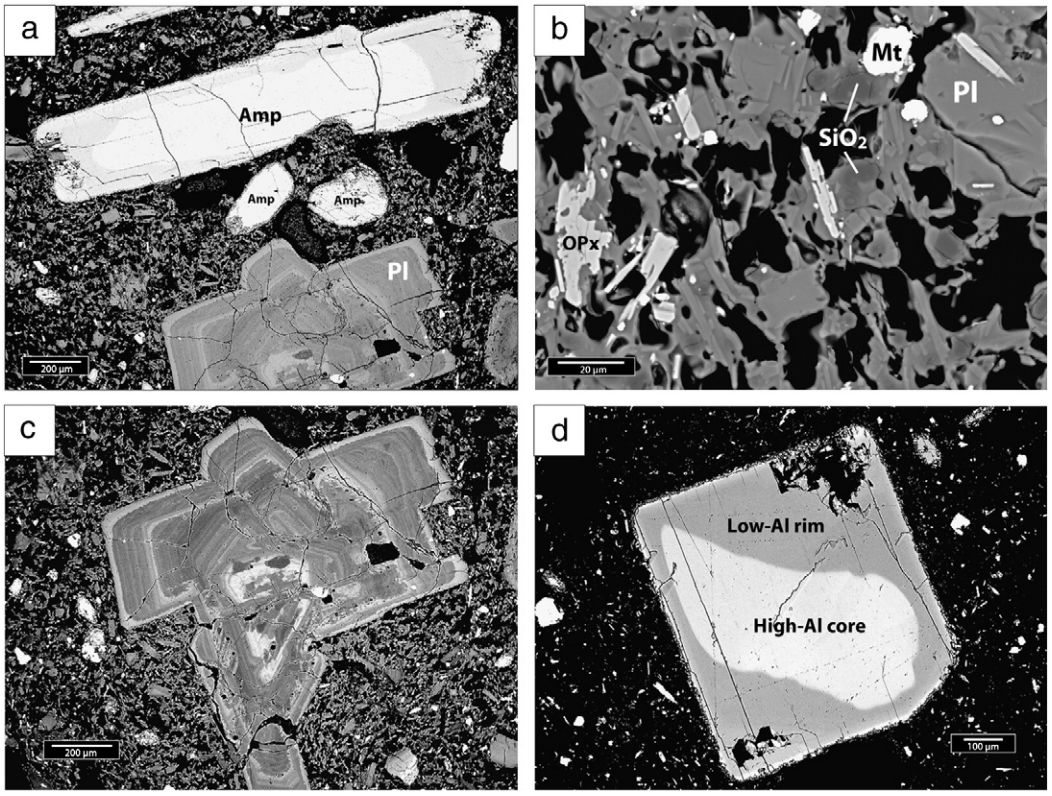

Fig. 1. Back-scatter electron (BSE) images of 1956 andesite: a — general view of the 1956 andesite showing abundant plagioclase and amphibole phenocrysts surrounded by vesiculated ground mass; b — groundmass composed of plagioclase, orthopyroxene, and Fe–Ti oxides; c — oscillatory-zoned plagioclase phenocrys; d — amphibole phenocryst with high-Al unhedral core (bright inner area) and low-Al rim. Pl — plagioclase, Amp — amphibole, Mt — magnetite, SiO_2 — silica phase, OPx — orthopyroxene.

Table 3
Composition of matrix glass and glassy melt inclusions in plagioclase.

	SiO2	TiO2	Al2O3	FeO	MgO	CaO	Na2O	K2O	Total[a]
	Matrix glass								
	77.94	0.47	9.82	2.10	1.63	1.04	3.04	3.61	98.80
	76.41	0.39	12.24	1.30	0.58	2.04	3.67	3.19	99.19
	78.61	0.11	11.44	1.01	0.12	0.62	3.55	4.32	98.83
	76.24	0.43	11.10	2.37	1.41	0.98	3.08	4.11	98.38
	75.20	0.18	13.66	1.15	0.10	2.12	3.64	3.75	99.41
	74.30	0.19	14.31	0.99	0.10	2.27	3.97	3.80	98.91
	77.56	0.23	12.04	1.20	0.15	1.05	3.52	4.15	98.46
	79.23	0.49	11.00	0.91	0.15	0.72	3.20	4.09	98.45
	75.56	0.46	13.61	0.76	0.12	2.20	3.93	3.23	100.05
Mean	76.78	0.33	12.14	1.31	0.48	1.45	3.51	3.81	98.94
SD	1.65	0.15	1.48	0.55	0.61	0.69	0.34	0.40	0.54
	Melt inclusions								
	74.22	0.29	13.64	1.20	0.13	2.10	4.26	3.92	99.36
	75.55	0.35	12.92	1.87	0.29	2.20	4.17	2.39	97.53
	75.81	0.47	12.93	1.82	0.29	2.21	3.86	2.46	96.14
	73.05	0.22	15.56	1.30	0.32	2.59	4.17	2.47	97.62
	75.09	0.22	14.26	1.83	0.32	2.41	3.04	2.63	97.92
	74.60	0.16	13.49	2.32	0.36	2.25	3.88	2.73	97.94
	73.27	0.07	14.13	1.69	0.44	2.85	3.81	3.56	97.66
Mean	74.51	0.25	13.85	1.72	0.31	2.37	3.89	2.88	97.74
SD	1.07	0.13	0.92	0.38	0.09	0.27	0.41	0.61	0.94

[a] All analyses normalized to 100%. Original totals are reported in the last column. Mn content is not reported.

3.19 to 4.32 with a mean of 3.92 wt.%. Al_2O_3, CaO, and Na_2O are negatively correlated with SiO_2 content, while other major components do not vary systematically (Fig. 3). The majority of melt inclusions are found in plagioclase phenocrysts near dissolution boundaries or within dusty zones. All melt inclusions are glassy. Composition of melt inclusions is slightly less silicic than matrix glass, varying from 73.3 to 75.8 with a mean value of 74.5 wt.%. K_2O varies from 2.39 to 3.92 with a mean value of 2.88 wt.% (Fig. 3, Table 3). Based on ion-probe measurements by Neill et al. (in prep), the concentrations of H_2O and CO_2 in 1956 Bezymianny melt inclusions average 2.4 ± 0.9 wt.% and 174 ± 63 ppm, respectively, which overlaps considerably with H_2O and CO_2 values for melt inclusions from 2007 eruptive products (Shcherbakov et al., 2011).

4. Experimental results

The distribution of mineral phases in the glass matrix was homogeneous across all experimental runs. The shapes of newly-grown phases were euhedral (Fig. 2a and b). Compositions of plagioclase microlites and outermost rims of larger crystals were homogeneous, overlapped considerably in individual experimental runs, and varied systematically with temperature and pressure, as discussed below. Compositions of groundmass glasses in individual experimental runs were homogeneous; they varied systematically with the temperature and pressure of different experimental runs. Quench textures were not observed in any of our experiments.

Simultaneous crystallization of plagioclase, orthopyroxene, clinopyroxene, magnetite, and amphibole was reproduced in experimental runs at a temperature range of 775–1100 °C and a pressure range of 50–200 MPa (Table 2). Experimental phase relationships are presented in Fig. 4. The magnetite field of stability is not shown, though opaque Fe–Ti oxides were identified in many experimental runs (Table 2). Orthopyroxene was the first phase to crystallize within the investigated pressure range. At pressure ≤150 MPa orthopyroxene crystallization was followed by plagioclase, while at pressures >150 MPa clinopyroxene crystallization preceded that of plagioclase. Amphibole was stable in experimental runs at pressures higher than 150 MPa and temperatures below 900 °C.

The amphibole–plagioclase–orthopyroxene mineral assemblage found in 1956 rocks was reproduced at 775 °C and 200 MPa. At 850 °C and 200 MPa two pyroxenes, plagioclase, and amphibole were stable, this also matched the natural assemblage, considering that small amounts of clinopyroxene are present in natural samples. The clinopyroxene–orthopyroxene–plagioclase mineral assemblage found in natural groundmasses was reproduced across a relatively wide range of pressures and temperatures outside the amphibole field of stability (850–1000 °C and 50–150 MPa, Fig. 4).

Groundmass glass compositions in our experimental runs varied systematically with pressure and temperature (Table 4, Fig. 5). Concentrations of SiO_2 and K_2O increased, whereas concentrations of FeO, MgO, Al_2O_3, and CaO decreased as temperature decreased isobarically. Concentrations of SiO_2 and K_2O decreased, whereas concentrations of CaO, Al_2O_3, and MgO increased as pressure increased isothermally. Composition of synthesized plagioclases varied from 56.1 to 78.3 An mol. % (Table 4); higher temperature and higher pressure favored the crystallization of Ca-rich plagioclase (Fig. 6).

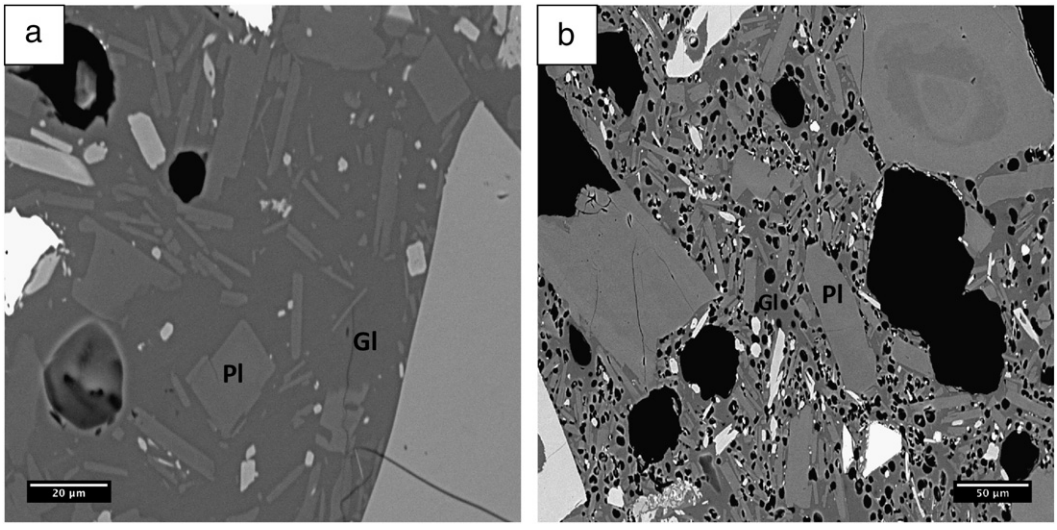

Fig. 2. Back-scatter electron (BSE) images of experimental run products. a — BZ-12 (950 °C, 50 MPa), b — BZ-1 (850 °C, 100 MPa).

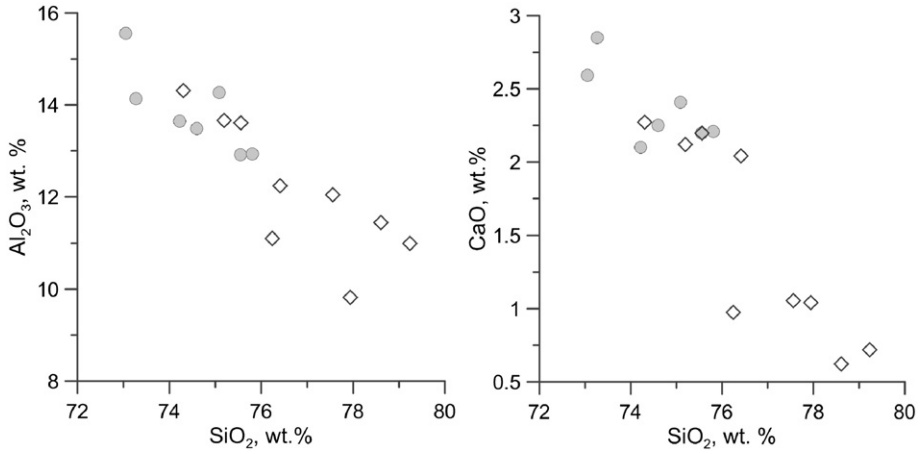

Fig. 3. CaO and Al_2O_3 versus SiO_2 variation diagrams from melt inclusions (circles) in plagioclase phenocrysts and matrix glass (diamonds).

5. Discussion

5.1. Attainment of equilibrium

Our experiments were designed to replicate the local equilibrium between melt and newly-grown crystalline phases, i.e. microlites and the outermost rims of phenocrysts, and therefore it is important to verify whether such equilibrium was attained. This is particularly relevant due to the short duration of our experimental runs, which was necessitated by the limited lifespan of the oxygen buffer assembly. Three lines of evidence suggest to us that local equilibrium was attained: (1) growth of new, euhedral crystalline phases (Fig. 2a and b), (2) compositional homogeneity of the newly-formed phases within individual experimental runs (Table 4), and (3) systematic changes in the composition of newly-grown phases (Figs. 5 and 6).

5.2. Pre-eruptive parameters for 1956 magma

While the 1956 Bezymianny magma does contain amphibole, the reaction rims indicate that amphibole is not stable at shallow levels within the Bezymianny magmatic system. Clinopyroxene microlites and microphenocrysts are present throughout natural 1956 samples, and therefore a phase assemblage of clinopyroxene, orthopyroxene, plagioclase, and Fe–Ti oxides seems more likely to represent the final stable phase assemblage of the 1956 Bezymianny magma. This phase assemblage was reproduced in experimental runs at temperatures from 850–1000 °C and pressures of 50–150 MPa (Fig. 4). At lower pressures (<100 MPa) the assemblage requires higher temperatures (900–1000 °C) to be reproduced than at higher pressures (850–950 °C).

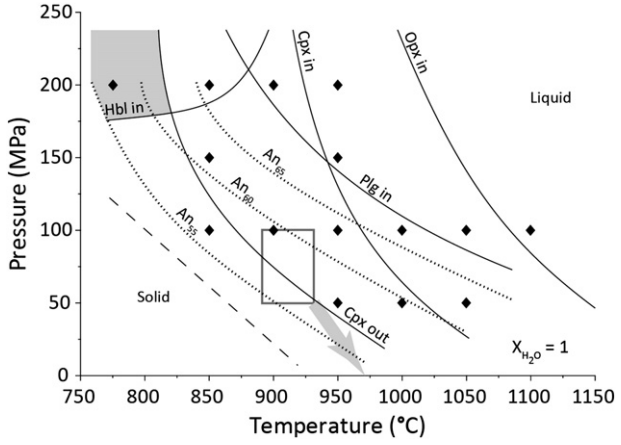

Fig. 4. Experimentally-determined phase relations for 1956 Bezymianny andesite. The grey area corresponds to deep magma storage where hornblende, plagioclase, orthopyroxene, and Fe–Ti oxides crystallize. The grey box outlines T-P conditions of last equilibration (890–930 °C and 50–100 MPa). The arrow points to T-P conditions of groundmass crystallization.

The pre-eruptive temperature of the 1956 magma was further constrained by Shipman and Gavrilenko (unpub. data) based on coexisting ilmenite-magnetite pairs from small, pumiceous juvenile clasts of the March 30, 1956 pyroclastic flow deposits. According to their results, the 1956 magma last equilibrated at 890–930 °C and oxygen fugacity of 0.5–1 log units above the NNO oxygen buffer. Comparing natural glass compositions to experimental compositions also imposes a constraint on the maximum pressure of final equilibration. The groundmasses of 1956 samples, even the most vesicular, are microlite rich, meaning that it is probable that groundmass compositions were modified syn-eruptively by decompression crystallization during ascent (cf. Plechov et al., 2008; Neill et al., 2010; Shcherbakov et al., 2011). Therefore we compare experimental glass compositions to both groundmass glass compositions and the compositions of melt inclusions, which represent liquid compositions entrapped prior to significant compositional modification by syn-eruptive crystallization. Experimental runs at pressures in excess of 100 MPa produce interstitial melts that are significantly less evolved (lower SiO_2 and K_2O, higher Al_2O_3 and CaO) than both groundmass glass compositions and melt inclusion compositions. As the compositions of these glasses and inclusions are only reproduced in experiments at pressures ≤100 MPa, this may be taken as an upper limit on the pressure at which the magma last equilibrated.

The combination of the temperature constraints from Fe–Ti oxide data and the maximum pressure limit imposed by groundmass glass compositions limits the pressure–temperature (P-T) range at which the 1956 Bezymianny magma last equilibrated to 890–930 °C and 50–100 MPa (Fig. 4). Based on an assumed overburden density of 2700 kg m^{-3}, these pressures correspond to depths of ~2–4 km below the Bezymianny edifice, which agrees reasonably well with the depth of a small magmatic storage region inferred from seismic data by Thelen et al. (2010). The pressure range also agrees well with, though it is slightly higher than pressures of melt inclusion entrapment inferred from H_2O-CO_2 solubility by Neill et al. (in prep). This not only strengthens our assertion that the magma last equilibrated at these low pressures prior to eruption, but that the magma was vapor-saturated prior to eruption.

5.3. Decompression processes associated with the 1956 eruption

Temperature and pressure in andesitic systems control residual melt composition in crystal-rich systems, which allows the pre-eruptive

Table 4
Glass and plagioclase compositions in experimental runs. Glass analyses are given on an anhydrous basis with VBD and totals reported separately.

Name	Conditions		SiO2	TiO2	Al2O3	FeO	MnO	MgO	CaO	Na2O	K2O	VBD	Total	Pl (% An) (SD)
BZ-1	850 °C 100 MPa	Mean	77.55	0.17	12.74	1.02	0.05	0.13	1.12	3.23	3.95	5.32	94.68	56.07 (0.89)
		SD	0.50	0.24	0.63	0.51	0.10	0.06	0.29	0.20	0.24	0.78	0.78	
BZ-2	775 °C 200 MPa	Mean	77.05	0.16	13.19	1.18	0.04	0.22	1.85	3.52	2.75	7.41	92.59	56.58 (1.5)
		SD	0.32	0.10	0.22	0.13	0.06	0.03	0.19	0.25	0.12	0.84	0.84	
BZ-3	1000 °C 100 MPa	Mean	67.95	0.65	15.32	4.55	0.12	1.39	4.14	3.85	1.98	3.59	96.41	65.14 (0.04)
		SD	0.92	0.18	0.27	0.54	0.06	0.24	0.28	0.14	0.10	0.57	0.57	
BZ-4	950 °C 100 MPa	Mean	72.87	0.41	13.93	2.79	0.09	0.75	2.79	3.87	2.44	3.88	96.12	60.14 (0.61)
		SD	0.71	0.14	0.32	0.32	0.09	0.18	0.17	0.15	0.10	0.38	0.38	
BZ-7	1100 °C 100 MPa	Mean	61.68	0.84	16.70	6.13	0.15	3.17	6.42	3.54	1.32	2.85	97.15	–
		SD	1.14	0.28	0.48	0.72	0.08	0.43	0.51	0.24	0.09	0.54	0.54	
BZ-9	1050 °C 100 MPa	Mean	64.73	0.91	17.11	4.12	0.15	2.45	5.23	3.57	1.68	4.80	95.20	–
		SD	0.60	0.31	0.17	0.28	0.09	0.09	0.42	0.17	0.09	0.77	0.77	
BZ-10	1000 °C 50 MPa	Mean	73.24	0.42	13.53	3.05	0.11	0.78	2.86	3.40	2.56	2.64	97.36	60.70 (1.33)
		SD	1.02	0.30	0.33	0.64	0.05	0.09	0.15	0.09	0.16	0.74	0.74	
BZ-11	1050 °C 50 MPa	Mean	68.93	0.51	14.67	4.48	0.13	1.47	4.09	3.58	2.09	2.79	97.21	60.33 (2.65)
		SD	1.04	0.21	0.34	0.35	0.07	0.12	0.51	0.16	0.15	0.80	0.80	
BZ-12	950 °C 50 MPa	Mean	76.34	0.28	12.63	2.01	0.07	0.38	2.00	3.36	2.89	2.98	97.02	57.99 (1.86)
		SD	1.04	0.26	0.68	0.33	0.08	0.10	0.31	0.12	0.13	0.73	0.73	
BZ-14	900 °C 100 MPa	Mean	76.92	0.38	12.64	1.85	0.05	0.32	1.97	3.16	2.65	3.58	96.42	58.72 (3.33)
		SD	0.72	0.31	0.39	0.18	0.06	0.13	0.25	0.17	0.14	0.55	0.55	
BZ-17	850 °C 150 MPa	Mean	71.65	0.39	14.94	2.81	0.06	0.84	3.47	3.53	2.25	5.08	94.92	63.24 (1.7)
		SD	0.50	0.23	0.22	0.20	0.07	0.04	0.17	0.22	0.08	0.65	0.65	
BZ-18	950 °C 150 MPa	Mean	64.65	0.88	16.34	5.13	0.15	1.99	5.38	3.63	1.80	4.90	95.10	68.69 (0.17)
		SD	0.35	0.36	0.20	0.20	0.04	0.04	0.11	0.14	0.06	0.56	0.56	
BZ-19	850 °C 200 MPa	Mean	70.69	0.35	15.77	2.86	0.05	0.76	3.74	3.52	2.20	8.18	91.82	66.71 (0.78)
		SD	0.37	0.21	0.23	0.30	0.06	0.10	0.20	0.24	0.10	0.55	0.55	
BZ-20	900 °C 200 MPa	Mean	67.24	0.48	16.29	4.02	0.13	1.48	4.82	3.54	1.95	6.39	93.61	78.29 (2.13)
		SD	0.34	0.29	0.27	0.27	0.05	0.12	0.07	0.20	0.06	0.67	0.67	
BZ-21	950 °C 200 MPa	Mean	63.86	0.56	17.20	4.73	0.11	2.30	5.99	3.60	1.59	5.44	94.56	–
		SD	0.35	0.23	0.16	0.15	0.04	0.06	0.25	0.20	0.06	0.33	0.33	

VBD — volatiles by difference.

parameters of magma storage to be estimated by comparing compositions of experimentally synthesized melt with melt inclusions and matrix glass (e.g. Rutherford et al., 1985), which together trace the evolution of groundmass melt composition during syn-eruptive crystallization (e.g. Blundy and Cashman, 2001; Brugger et al., 2003; Blundy and Cashman, 2005). In the case of Bezymianny, melt inclusions match experimental melt produced at 50–100 MPa assuming a temperature of 890–930 °C (Fig. 5). More evolved matrix glass compositions match experimental melt compositions at pressures ≤50 MPa. Low-pressure pre-eruptive magma storage is supported by other petrological observations, such as amphibole breakdown rims and volatiles content in melt inclusions. Development of breakdown rims is usually attributed to magma storage conditions that are lower in pressure than those at which amphibole is stable. For Bezymianny andesite, amphibole is stable at ≥150–200 MPa (Fig. 4), and therefore breakdown rims suggest magma storage at pressures lower than 150–200 MPa. Ion probe analyses of melt inclusions in plagioclase and orthopyroxene phenocrysts from the 1956 eruption yielded values of 2.4 ± 0.9 wt.% H_2O and 174 ± 64 ppm CO_2 (Neill et al., in prep). According to the solubility model of Newman and Lowenstern (2002) the determined H_2O and CO_2 concentrations correspond to an entrapment pressure of ~75 MPa, assuming fluid saturation.

Potassium and water content in melt inclusions and matrix glass may be used to calculate the evolution of magma crystallinity as a function of pressure, assuming incompatible behavior of K and H_2O saturation in the melt (e.g. Cashman, 1992). Melt inclusions and matrix glass indicate that magma evolves toward increasing crystallinity at lower pressures (Fig. 7). At 100–120 MPa the magma contains 45–50 wt.% of crystals, while at 50 MPa the average crystallinity increases to 55–60 wt.%. Matrix glasses represent highly crystalline (up to 70 wt.% crystals) material equilibrated at pressure ≤20 MPa. Since amphibole is present in the system, K may not behave incompatibly. To verify whether our calculations based on the K content underestimate crystallinity due to the presence of amphibole, we performed similar calculations using Rb concentrations (Turner et al., 2013) in bulk rock and Rb and H_2O concentrations in melt inclusions measured by SHRIMP (Neill et al., in prep). Although K-based calculations yield systematically lower crystal content values than Rb-based calculations do, their results overlap considerably (Fig. 7). Such a pattern, with negative correlations between crystal content and pressure, is best explained by decompression-driven crystallization in response to magma ascent, and has been described for other andesitic volcanoes (e.g. Cashman, 1992; Blundy and Cashman, 2001; Hammer and Rutherford, 2002; Brugger et al., 2003; Blundy et al., 2006; Brugger and Hammer, 2010). Wide deviations in crystal content at lower pressures might suggest different ascent rates; magma degassing outpaces crystallization due to kinetic restrictions on crystal nucleation and growth at high decompression rates, while at lower decompression rates, the crystallization response to degassing is more complete (Martel and Schmidt, 2003; Brugger and Hammer, 2010).

By applying the plagioclase-melt model of Putirka (2005) to melt inclusion compositions, we reconstructed plagioclase liquidus temperature as a function of pressure. Melt inclusions entrapped at pressure ≥80 MPa indicate temperatures ~850 °C, while at lower pressure the temperature rises to ~950 °C (Fig. 7). Although absolute temperature estimates may be influenced by boundary layer effects and post-entrapment crystallization of melt inclusions, our results appear to be consistent with temperatures determined previously (Kadik et al., 1986; Almeev et al., 2002; Plechov et al., 2008).

5.4. Timescales of shallow magma storage

Below stability field pressures, amphibole starts to react with a melt and decomposes to an aggregate of anhydrous minerals (generally pyroxene, plagioclase, and Fe–Ti oxides). The width of breakdown rims has been experimentally calibrated as a function of time spent out of the amphibole stability field (Rutherford and Hill, 1993; Browne

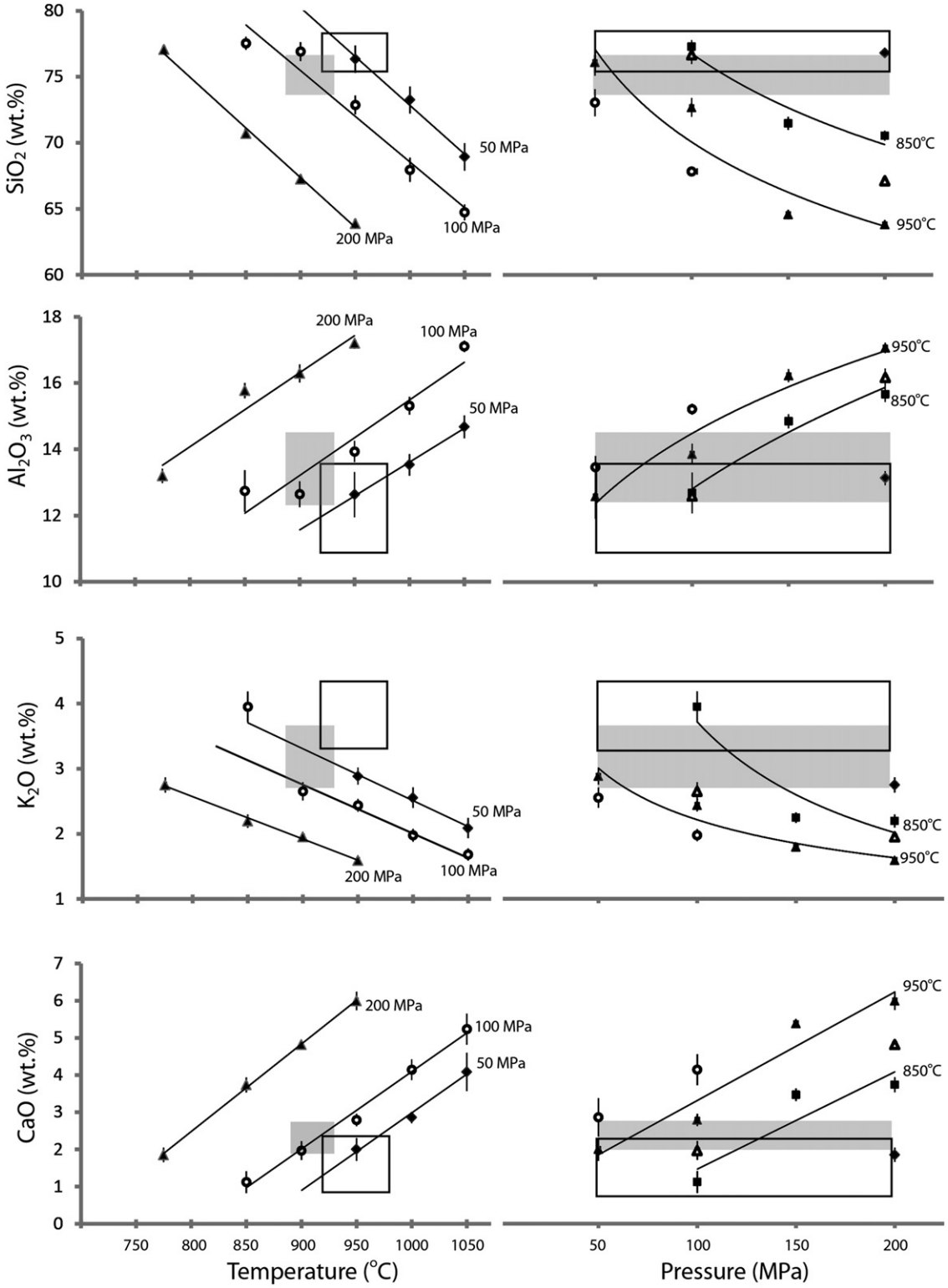

Symbols on Temperature - wt.% graphs

- 50 MPa
- 100 MPa
- 200 MPa

Symbols on Pressure- wt.% graphs

- 775 °C
- 850 °C
- 900 °C
- 950 °C
- 1000 °C

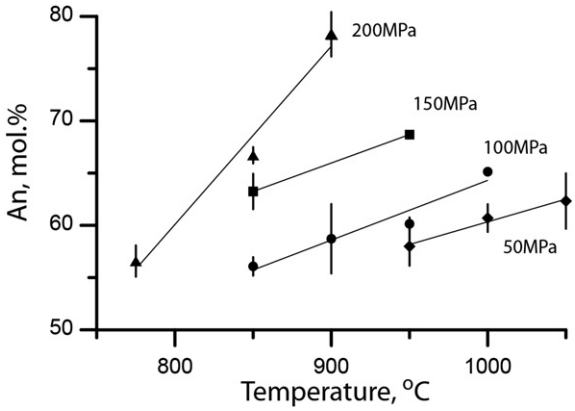

Fig. 6. Variations of experimental plagioclase compositions as a function of temperature and pressure.

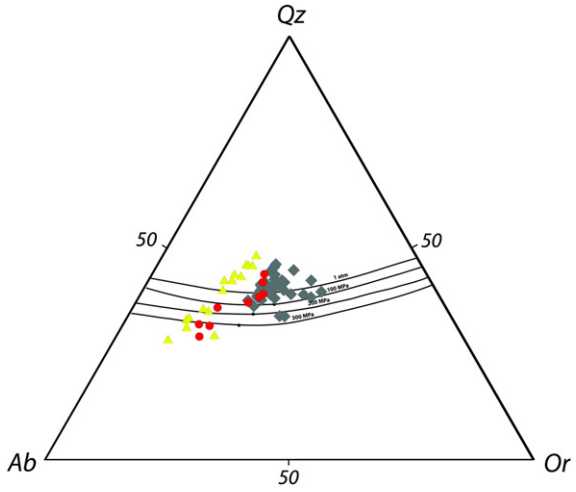

Fig. 8. Q-Ab-Or projection of melt inclusions in phenocryst (triangles) and matrix glass (circles) compositions in pyroclastic flow deposits, and groundmass glass composition in cryptodome samples (diamonds) from Neill et al. (2010). Q-Ab-Or projection after Blundy and Cashman (2001), with cotectics after Brugger et al. (2003).

and Gardner, 2006). Using the experimental data of Rutherford and Hill (1993), the formation time of 5–10 μm breakdown rims for pyroclastic and 25–35 μm rims for cryptodome deposits can be estimated as 2–14 and 4–34 days, respectively. Cryptodome samples, however, are highly crystalline and degassed (Neill et al., 2010), which suggests that diffusion processes in cryptodome melt, which will control the growth of

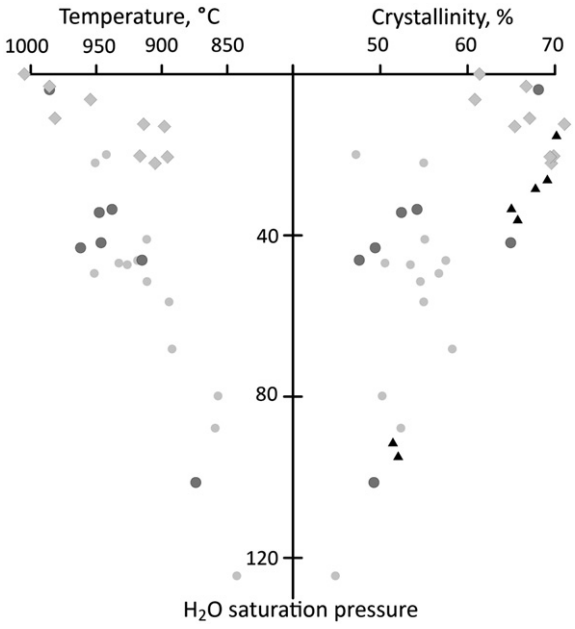

Fig. 7. Variations of temperature and crystal content of magma as a function of pressure calculated based on H_2O, K, and Rb concentrations on melt inclusions and matrix glass (see Discussion section). Large dark grey circles — melt inclusions in plagioclase of 1956 pyroclastic flow deposits, calculated based on EMPA analyses of K concentration and H_2O determined by volatiles by difference (VBD); small light grey circles — melt inclusions in plagioclase of 1956 cryptodome rocks; triangles — melt inclusions in plagioclase of 1956 pyroclastic flow deposits, calculated based on SHRIMP analyses of Rb and H_2O (Neill et al., in prep); diamonds — matrix glass of 1956 pyroclastic flow deposits.

breakdown rims, are much slower than in volatile-rich magmas stored at depth. Therefore, estimations of rim growth time for cryptodome samples given in Plechov et al. (2008) are likely underestimates.

Another way to determine timescales of crystallization is by the kinetics of groundmass crystallization. Melt inclusion compositions can be characterized using the ternary Q-Ab-Or system (Tuttle and Bowen, 1958), the projection scheme of Blundy and Cashman (2001), and the cotectics of Brugger et al. (2003), and generally follow a decompression crystallization pattern (Fig. 8, Blundy and Cashman, 2001). As it reaches 1 atm cotectic, a silica phase should appear on liquidus, though due to the exceptionally slow kinetics of crystal nucleation at low pressures and low melt H_2O contents (Brugger et al., 2003), crystallization of the silica phase may be delayed, and therefore glass compositions may evolve past the 1 atm cotectic. In decompression experiments on rhyolithic magmas, Brugger and Hammer (2010) observed no silica phase crystallization in experiments shorter than 208 h, and only found silica in experiments held at final pressure for 1000–1200 h. Assuming that the groundmass melt compositions were similar to the rhyolite compositions of the Brugger and Hammer (2010) experiments, the presence of a silica phase in Bezymianny samples indicates that the magma was stored at shallow depth for longer than 1000–1200 h (40 days).

The aforementioned methods of estimating timescales provide no more than estimates, but they do lend themselves to certain inferences. Samples from the 1956 Bezymianny pyroclastic flow deposits represent magma that reached shallow depths a few days to several weeks prior to the 1956 eruption. By contrast, magma stored within the 1956 cryptodome likely ascended much earlier.

6. Conclusions

Comparison of experimentally synthesized and natural Bezymianny Volcano melts indicates that magma was last and transiently stored at 50–100 MPa (1.5–3 km below the summit) and 890–930 °C prior to the 1956 eruption. Melt inclusion compositions exhibit a negative correlation between volatiles and potassium content, interpreted as a result of decompression-driven crystallization. As the 1956 magma ascended, its temperature and crystallinity rose from ~850 °C and ~45% at ~100–120 MPa, to ~950 °C and 50–60% at ~40 MPa. Timescales of shallow magma storage, estimated based on amphibole breakdown rims and kinetics of crystallization in rhyolitic melts, are estimated as al least 40 days.

Fig. 5. Variations in experimental groundmass glass compositions as a function of temperature and pressure. Shaded areas and black boxes show average compositions of melt inclusions and matrix glass, respectively ($\pm 1\sigma$). On the T-composition diagrams, shaded areas and black boxes are limited along the x axis according temperature estimates for melt inclusions and matrix glass, given in the text.

Acknowledgements

We highly appreciate help and support by Jessica Larsen while conducting experiments in her Experimental Petrology Laboratory, UAF. Electron microprobe analyses were performed at the Advanced Instrumentation Laboratory, UAF of UAF, under the direction of Ken Severin. Numerous discussions with Alexander Maximov, Steve Turner, Theresa Kayzar, Jill Shipman, Max Gavrilenko, and other PIRE-Kamchatka project participants were always inspiring and motivating. Detailed, constructive, and highly encouraging reviews by Bruno Scaillet and Renat Almeev significantly improved the article. Funding for this work was provided by the NSF PIRE — Kamchatka Award OISE 0530278.

References

Almeev, R.R., Ariskin, A.A., Ozerov, A.Y., 2002. Problems of the stoichiometry and thermobarometry of magmatic amphiboles: an example of hornblende from the andesites of Bezymyannyi volcano, eastern Kamchatka. Geochemistry International 40 (8), 723–738.

Belousov, A.B., 1996. Deposits of the 30 March 1956 directed blast at Bezymianny Volcano, Kamchatka, Russia. Bulletin Volcanologique 57, 649–662.

Belousov, A.B., Voight, B., Belousova, M.G., 2007. Directed blasts and blast-currents: a comparison of the Bezymianny 1956, Mount St Helens 1980, and Soufriere Hills, Montserrat 1997 eruptions and deposits. Bulletin Volcanologique 69, 701–740.

Blundy, J., Cashman, K.V., 2001. Ascent-driven crystallisation of dacite magmas at Mount St Helens, 1980–1986. Contributions to Mineralogy and Petrology 140, 631–650.

Blundy, J., Cashman, K.V., 2005. Rapid decompression-driven crystallization recorded by melt inclusions from Mount St. Helens volcano. Geology 33 (10), 793–796.

Blundy, J., Cashman, K.V., Humphreys, M.C.S., 2006. Magma heating by decompression-driven crystallization beneath andesite volcanoes. Nature 443, 76–80.

Browne, B.L., Gardner, J.E., 2006. The influence of magma ascent path on the texture, mineralogy, and formation of hornblende reaction rims. Earth and Planetary Science Letters 246 (3–4), 161–176.

Browne, B., Izbekov, P., Eichelberger, J., Churikova, T., 2010. Pre-eruptive storage conditions of the Holocene dacite erupted from Kizimen Volcano, Kamchatka. International Geology Review 52 (1), 95–110.

Brugger, C.R., Hammer, J.E., 2010. Crystallization kinetics in continuous decompression experiments: implications for interpreting natural magma ascent processes. Journal of Petrology 51 (9), 1941–1965.

Brugger, C.R., Johnston, A.D., Cashman, K.V., 2003. Phase relations in silicic systems at one-atmosphere pressure. Contributions to Mineralogy and Petrology 146, 356–369.

Cashman, K.V., 1992. Groundmass crystallization of Mount St. Helens dacite, 1980–1986: a tool for interpreting shallow magmatic processes. Contributions to Mineralogy and Petrology 109, 431–449.

Cottrell, E., Gardner, J.E., Rutherford, M.J., 1999. Petrologic and experimental evidence for the movement and heating of the pre-eruptive Minoan rhyodacite (Santorini, Greece). Contributions to Mineralogy and Petrology 135, 315–331.

Devine, J.D., Gardner, J.E., Brack, H.P., Layne, G.D., Rutherford, M.J., 1995. Comparison of microanalytical methods for estimating H_2O contents of silicic volcanic glasses. American Mineralogist 80 (3–4), 319–328.

Donovan, J.J., Kremser, D., Fournelle, J.H., 2007. Probe for Windows User's Guide and Reference, Enterprise edition. Probe Software, Inc., Eugene.

Fedotov, S.A., Zharinov, N.A., Gontovaya, L.I., 2010. The magmatic system of the Klyuchevskaya Group of Volcanoes inferred from data on its eruptions, earthquakes, deformation, and deep structure. Journal of Volcanology and Seismology 4 (1), 1–33.

Gardner, J.E., Rutherford, M., Carey, S., Sigurdsson, H., 1995. Experimental constraints on pre-eruptive water contents and changing magma storage prior to explosive eruptions of Mount St Helens Volcano. Bulletin Volcanologique 57, 1–17.

Geschwind, C.-H., Rutherford, M.J., 1992. Cummingtonite and the evolution of the Mount St. Helens (Washington) magma system: an experimental study. Geology 20, 1011–1014.

Girina, O.A., 2013. Chronology of Bezymianny Volcano activity, 1956–2010. Journal of Volcanology and Geothermal Research. 263, 21–40.

Gorshkov, G.S., Bogoyavlenskaya, G.E., 1965. Bezymianny Volcano and the features of its 1955–1963 eruption. Nauka, Moscow (in Russian).

Hammer, J.E., Rutherford, M.J., 2002. An experimental study of the kinetics of decompression induced crystallization in silicic melt. Journal of Geophysical Research 107 (B1), 2021.

Izbekov, P., Gardner, J.E., Eichelberger, J.C., 2004. Comagmatic granophyre and dacite from Karymsky volcanic center, Kamchatka: experimental constraints for magma storage conditions. Journal of Volcanology and Geothermal Research 131 (1–2), 1–18.

Kadik, A.A., Maksimov, A.P., Ivanov, A.P., 1986. Physico-chemical crystallization conditions and genesis of andesites. Nauka, Moscow (in Russian).

Larsen, J.F., 2006. Rhyodacite magma storage conditions prior to the 3430 yBP caldera-forming eruption of Aniakchak volcano, Alaska. Contributions to Mineralogy and Petrology 152, 523–540.

Martel, C., Schmidt, B.C., 2003. Decompression experiments as an insight into ascent rates of silicic magmas. Contributions to Mineralogy and Petrology 144, 397–415.

Neill, O.K., Hammer, J.E., Izbekov, P.E., Belousova, M.G., Belousov, A.B., Clarke, A.B., Voight, B., 2010. Influence of pre-eruptive degassing and crystallization on the juvenile products of laterally directed volcanic explosions. Journal of Volcanology and Geothermal Research 198, 264–274.

Newman, S., Lowenstern, J.B., 2002. VolatileCalc: a silicate melt–H2O–CO2 solution model written in Visual Basic for excel. Computers & Geosciences 28 (5), 597–604.

Nielsen, C.H., Sigurdsson, H., 1981. Quantitative methods for electron micro-probe analysis of sodium in natural and synthetic glasses. American Mineralogist 66 (5–6), 547–552.

Ozerov, A.Yu., Ariskin, A.A., Kyle, Ph., Bogoyavlenskaya, G.E., Karpenko, S.F., 1997. Petrological-geochemical model for genetic relationships between basaltic and andesitic magmatism of Klyuchevskoi and Bezymyannyi volcanoes, Kamchatka. Petrology 5 (6), 614–635.

Pichavant, M., Costa, F., Burgisser, A., Scaillet, B., Martel, C., Poussineau, S.P., 2007. Equilibration scales in silicic to intermediate magmas - implications for experimental studies. Journal of Petrology 48, 1955–1972.

Plechov, P., Tsai, A., Shcherbakov, V., Dirksen, O., 2008. Opacitization conditions of hornblende in Bezymyannyi Volcano andesites (March 30, 1956 eruption). Petrology 16 (1), 19–35.

Putirka, K.A., 2005. Igneous thermometers and barometers based on plagioclase plus liquid equilibria: tests of some existing models and new calibrations. American Mineralogist 90 (2–3), 336–346.

Roman, D.C., Cashman, K.V., Gardner, C.A., Wallace, P.J., Donovan, J.J., 2006. Storage and interaction of compositionally heterogeneous magmas from the 1986 eruption of Augustine Volcano, Alaska. Bulletin Volcanologique 68, 240–254.

Rutherford, M.J., Devine, J.D., 1996. Pre-eruption pressure-temperature conditions and volatiles in the 1991 dacitic magma of Mount Pinatubo. In: Newhall, C., Punongbayan, R. (Eds.), Fire and Mud: Eruptions and lahars of Mount Pinatubo, Phillipines. Univ. of Wash. Press, Seattle, WA, pp. 751–766.

Rutherford, M.J., Hill, P.M., 1993. Magma ascent rates from amphibole breakdown: an experimental study applied to the 1980–1986 Mount St. Helens eruptions. Journal of Geophysical Research 98, 19667–19685.

Rutherford, M.J., Sigurdsson, H., Carey, S., Davis, A., 1985. The May 18, 1980, Eruption of Mount St. Helens: 1. Melt composition and experimental phase equilibria. Journal of Geophysical Research 90 (B4), 2929–2947.

Scaillet, B., Evans, B.W., 1999. The 15 June 1991 eruption of Mount Pinatubo. I. Phase equilibria and pre-eruption P-T-f_{O2}-f_{H2O} conditions of the dacite magma. Journal of Petrology 40 (3), 381–411.

Shcherbakov, V.D., Plechov, P.Yu., Izbekov, P.E., Shipman, J.S., 2011. Plagioclase zoning as an indicator of magma processes at Bezymianny Volcano, Kamchatka. Contributions to Mineralogy and Petrology 162, 83–99.

Thelen, W., West, M., Senyukov, S., 2010. Seismic characterization of the fall 2007 eruptive sequence at Bezymianny Volcano, Russia. Journal of Volcanology and Geothermal Research 194, 201–213.

Turner, S.J., Izbekov, P., Langmuir, C., 2013. The magma plumbing system of Bezymianny Volcano: Insights from a 54 year time series of trace element whole-rock geochemistry and amphibole compositions. Journal of Volcanology and Geothermal Research. 263, 107–120.

Tuttle, O.F., Bowen, N.L., 1958. Origin of granite in the light of experimental studies in the system $NaAlSi_3O_8$–$KAlSi_3O_8$–SiO_2–H_2O. Geo. Soc. Am., New York.